ON THE USE OF LYAPUNOV EXPONENTS TO DETECT GLOBAL PROPERTIES OF THE DYNAMICS

CARLES SIMÓ

Departament de Matemàtica Aplicada i Anàlisi, Universitat de Barcelona, Gran Via, 585, 08071 Barcelona (Spain)
E-mail: carles@maia.ub.es

Different methods have been proposed for the numerical computation of Lyapunov exponents. After a quick review we shall describe a new powerful method which is specially suitable to detect domains of ordered motions. Then several examples will be presented, applied to conservative and non-conservative systems, discrete and continuous. They show how one can obtain relevant information on the global dynamics in a fast way. Finally, an application to compute the metric entropy of a family of diffeomorphisms will be done. In that case to have an accurate value of the entropy is important to support different conjectures.

1. Computing Lyapunov exponents

Lyapunov exponents measure the mean value of the exponential rate of increase of the distance between nearby orbits (*growth factor*). For concreteness assume F is a diffeomorphism in an open set $\mathcal{U} \subset \mathbb{R}^d$ (one can also work in manifolds) with bounded orbits. Let $x_0 \in \mathcal{U}$ be an initial point and $x_n = F^n(x_0)$, $n \in \mathbb{Z}$ its orbit. Given a vector $\xi \in T_{x_0}\mathbb{R}^d$, $\|\xi\| = 1$ consider

$$\lim_{k\to\infty} \log(\|DF^n(x_0)\xi\|)/n. \tag{1}$$

The limit exists for almost all x_0 and ξ and, with probability 1, gives the *maximal Lyapunov exponent.* In fact, the first k Lyapunov exponents can be computed as follows with the algorithm that we describe now.

Let $\xi_0^j, 1 \leq j \leq k$ be random initial vectors. From them one can obtain orthonormal vectors, again denoted as ξ_0^j. Initialise $y_0^j = 0, 1 \leq j \leq k$. After m steps of the algorithm we do next one. The images

$$\eta_{m+1}^j = DF(x_0)\xi_m^j, \quad 1 \leq j \leq k$$

are computed and then *orthogonalised* (not yet normalised) to obtain vectors ζ_{m+1}^j. The values of the y numbers are updated by

$$y_{m+1}^j = y_m^j + \log(\|\zeta_{m+1}^j\|) \tag{2}$$

and, finally, $\xi^j_{m+1} = \zeta^j_{m+1}/\|\zeta^j_{m+1}\|, 1 \leq j \leq k$. Then the estimates of the first k Lyapunov exponents after n iterates are computed as

$$\ell^j_n = y^j_n/n, \quad 1 \leq j \leq k. \tag{3}$$

The values of ℓ^j_n converge to limits ℓ^j when $n \to \infty$ with probability 1. In particular ℓ^1 coincides with the result of (1).

However, this procedure has some difficulties that we discuss in the case $k=1$: (a) If $\ell^1=0$ the convergence can be too slow ($O(\log(n)/n)$); (b) For different values of n one can obtain quite different values of ℓ^1_n (think about a chaotic orbit of a symplectic map passing close to sticky tori); (c) The initial and final points, x_0, x_n, can be far away and give errors in the average (the growth factors can be very different along $\mathcal{U}$ in the regular case).

These difficulties can be decreased by using a slightly different, weighted, version of (2) and (3) which, using $\bar{y}^j_n = \sum_{k=1}^n y^j_k$, are replaced by

$$y^j_{m+1} = y^j_m + \log(\|\zeta^j_{m+1}\|)(m+1)^2, \quad \ell^j_n = 12\bar{y}^j_n/(n^4+4n^3+5n^2) - 2/n, \tag{4}$$

and one selects (on a given range of final values of n) the one which minimises $d(x_0, x_n)$ (see [7,3,5] and references therein, and [3] for variants of (4)).

In the case of flows the formulas are similar. Then the sums defining the values of $y^j(t)$ are replaced by integrals and $n \to \infty$ by $t \to \infty$. Alternatively, one can work with the map defined by the flow time-τ map, for a fixed τ (for instance, for τ-periodic vector fields). Note that the use of Poincaré maps has the problem of the different return times. Quasi-periodic time dependence can be studied using skew products, see Sect. 4.

Next we describe some examples which illustrate how useful can be the computation of Lyapunov exponents in quite different cases.

2. A first example: Scanning phase space and parameters

Consider a standard-like family of maps, without the entire character,

$$F_{\varepsilon,\mu,\varphi}\begin{pmatrix} x \\ y \end{pmatrix} = \begin{pmatrix} \bar{x} \\ \bar{y} \end{pmatrix} = \begin{pmatrix} x + \varepsilon\bar{y} \pmod{2\pi} \\ y + \varepsilon f_{\mu,\varphi}(x) \end{pmatrix}, \tag{5}$$

where φ breaks symmetry, $f_{\mu,\varphi}(x) = g_{\mu,\varphi}(x) - \bar{g}$, being $g_{\mu,\varphi}(x) = \frac{\sin(x+\varphi)}{1-\mu\cos(x)}$, $\bar{g} = \mathrm{av}(g)$. Scaling y by ε, the map is defined in $\mathbb{T}^2$. For $x_0 = 0, y_0 \in [0, 2\pi]$ different values of $\varepsilon \in [0,1]$ have been scanned, looking for regular ($\ell^1 = 0$) or chaotic ($\ell^1 > 0$) motion. See [4] for further information.

Figure 1 (left) shows some results for $\mu = 0.5$, $\varphi = 1$. In the horizontal (resp. vertical) axis the variable $y/(2\pi)$ (resp. ε) is shown. The white parts on top correspond to $\ell^1 > 0$, all other values having $\ell^1 = 0$. Additional information (using other methods) is displayed: Black lines, emerging from $\varepsilon = 0$, give the location of invariant curves, all points in a line having the same rotation number (of the form $m\gamma/100$, $1 \leq m \leq 161$, $\gamma = (\sqrt{5}-1)/2$). Dark grey domains correspond to resonant zones and zones of islands inside the 1:1 and 1:2 resonances. These two resonances are shown in light grey.

Further examples (for flows and for non-conservative cases) can be found in [7,3,2]. In all cases, the Lyapunov exponents give a clear evidence of the properties of the dynamics.

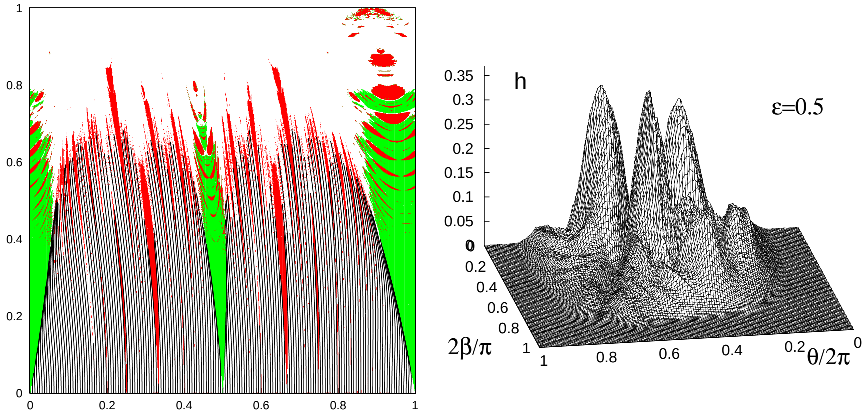

Figure 1. Left: An illustration of the stability properties of the map (5). Right: Values of the metric entropy, $h = h_{\varepsilon,\theta,\beta}$, for the map (6) as a function of β, θ for $\varepsilon = 0.5$ corrected by the factor $\cos(\beta)(1-\cos(\theta))$. See the text for details.

3. Metric entropy

In [5] the following family of area-preserving maps in $\mathbb{S}^2$ is studied

$$F_{\varepsilon,g}(x,y,z) = g \circ T_\varepsilon(x,y,z), \qquad x^2+y^2+z^2 = 1, \tag{6}$$

where T_ε denotes a twist around the z-axis which rotates by $\pi\varepsilon(z+1)$ the points on a given z plane. The map g is an element of $SO(3)$, which can be identified with a rotation of angle θ around the axis of latitude β and longitude λ (λ is irrelevant). One considers $SO(3)$ with the Haar measure μ, which has a density σ proportional to $\cos(\beta)(1-\cos(\theta))$.

For given $\varepsilon, \theta, \beta$ we can compute the maximal Lyapunov exponent $\ell^1(p)$ for the points p on S^2. The metric entropy $h_{\varepsilon,\theta,\beta}$ of the map $F_{\varepsilon,g}$ is computed by integrating $\ell^1(p)$ with respect to the usual measure in $\mathbb{S}^2$. For small ε this is a major task due to the wild behaviour of $\ell^1(p)$ with respect to p. Fig.1 (right) shows the strong dependence of $h \times \sigma$ on (θ, β) for $\varepsilon = 0.5$.

Finally we can compute an average entropy of the family, for a fixed ε as

$$\Lambda(\varepsilon) = \int_{SO(3)} h_{\varepsilon,\theta,\beta} d\mu. \tag{7}$$

Figure 2 (left) shows the estimated values of $\Lambda(\varepsilon)$ for small ε. Note that it is a clear indication of behaviour exponentially small with respect to ε.

On the other hand we can compute the entropy of the *randomised map*. This means that the map whose differential is applied to the vector ξ_n^1 is of the form $g_n \circ T_\varepsilon$, where the g_n are taken successively at random in $SO(3)$ with respect to μ. It is known that the process converges with probability 1 to some value, $R(\varepsilon)$ which can be computed explicitly

$$R(\varepsilon) = \int_0^{\frac{1}{2}} \log(1 + (2\pi\varepsilon x(1-x))^2)dx. \tag{8}$$

See [5] for motivation and details. It was conjectured that $\Delta(\varepsilon) = \Lambda(\varepsilon) - R(\varepsilon)$ could be positive. This would have quite interesting consequences, and it is true for some families of linear maps. For small values of ε this conjecture is not true (from (8) $R(\varepsilon) = O(\varepsilon^2)$ around $\varepsilon = 0$), but Fig. 2 (right) gives evidence that it can be true for large ε. As then $\Delta(\varepsilon)$ becomes small, very good estimates are needed to obtain $\ell^1(p)$, then $h_{\varepsilon,\theta,\beta}$ and, finally, in (7).

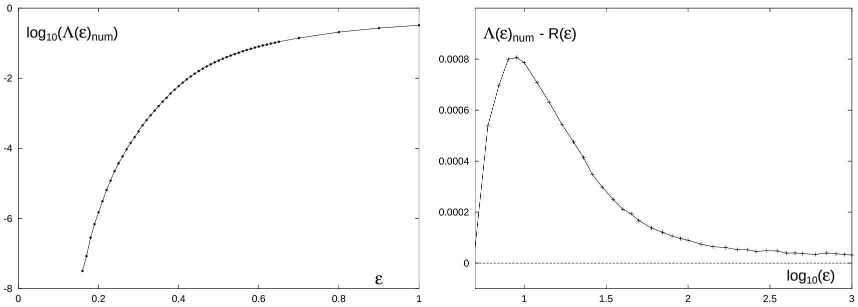

Figure 2. Left: Values of $\Lambda(\varepsilon)_{\mathrm{num}}$ for ε small. Right: The small difference $\Lambda(\varepsilon)_{\mathrm{num}} - R(\varepsilon)$ for ε large. See the text for details.

4. Linear differential equations with quasi-periodic coefficients

Now consider a linear differential equation in $\mathbb{R}^n$

$$\dot{x} = A(\theta_1, \theta_2), \qquad \text{where} \qquad \dot{\theta}_1 = \omega_1, \qquad \dot{\theta}_2 = \omega_2, \tag{9}$$

ω_1, ω_2 satisfying a Diophantine condition and A a matrix 2π-periodic in

(θ_1, θ_2). One can assume $\omega_1 = 1, \omega_2 = \omega$. Let $M_\varphi(t)$ be the solution of (9) with initial conditions $M_\varphi(0) = I, \theta_1(0) = 0, \theta_2(0) = \varphi$ and let $N(\varphi) = M_\varphi(2\pi)$. To study (9) is equivalent to study the skew product in $\mathbb{R}^n \times \mathbb{S}^1$

$$(x, \varphi) \mapsto (N(\varphi)x, \varphi + 2\pi\omega). \tag{10}$$

Matrix A is taken coming from a transformed Hamiltonian system

$$A(\theta_1, \theta_2) = \begin{pmatrix} 0 & I_2 \\ D & -2J_2 \end{pmatrix}, \quad I_2 = \begin{pmatrix} 1 & 0 \\ 0 & 1 \end{pmatrix}, \quad J_2 = \begin{pmatrix} 0 & 1 \\ -1 & 0 \end{pmatrix}, \quad D = \mathrm{diag}(f_1, f_2),$$

where $f_1 = \lambda_1(1 + \varepsilon\cos(\theta_2))$, $f_2 = \lambda_2(1 + \varepsilon\cos(\theta_1))$.

A value $\varepsilon = 1$ has been used, to be far away from the perturbation domain. As a 4D Hamiltonian, the case $\varepsilon = 0$ (or the case $\omega \in \mathbb{Q}$) can be, generically, of the form: elliptic-elliptic (EE) and then $\ell^1 = \ell^2 = 0$; elliptic-hyperbolic (EH) and then $\ell^1 > 0, \ell^2 = 0$; hyperbolic-hyperbolic (HH) and then $\ell^1 \geq \ell^2 > 0$; complex saddle (CS) and then $\ell^1 = \ell^2 > 0$.

Using $\lambda_2 = -4$ a range of λ_1 has been scanned with $\omega = \gamma^{-1} = (\sqrt{5}+1)/2$. If we use instead $\omega = q_k = F_{k+1}/F_k$ (F_k the kth Fibonacci number) then ℓ^1, ℓ^2 depend on the initial phase φ (the orbits of (10) are discrete in $\mathbb{S}^1$). Let us denote them as $\chi^j(\varphi)$. To recover continuity of ℓ^j with respect to ω one has to average χ^j with respect to φ. The behaviour is displayed in Fig. 3 (top). Only ℓ^2 is shown. For q_k close to γ^{-1} the variation of $\chi^1(\varphi)$ is small (uniform hyperbolicity). On the other hand $\chi^2(\varphi)$ reaches 0 in narrow domains for all q_k close to γ^{-1}. Assume we skip the hyperbolic part associated to ℓ^1. For $\omega = \gamma^{-1}$ the ℓ^2 shows (dense) resonance intervals (bumps in Fig. 3) which correspond to λ_1 for which (9) is reducible to constant coefficients. In the complement, where a rotation number changes while $\ell^2 > 0$, it is suggested that (9) is not reducible. Compare with Hill's case [1] far away from the perturbation domain.

For $\omega = \gamma^{-1}$ both ℓ^j are the integral of growth factors gf^j depending of φ. These factors are obtained from the $\log(\|\zeta^j_m\|)$ associated to the φ_m along the orbit after a transient (see (2) and (10)). For $\lambda_1 = -3.694$ (reducible) the gf^j are smooth, while for $\lambda_1 = -3.689$ (not reducible) gf^2 is wild (see Fig. 3 bottom).

Looking at the bumps of (the averaged) ℓ^2 for $\omega = q_k$ (Fig. 3 top) it has been observed that the periodic equation (in what concerns only ℓ^2) is either of H type or has a single interval of E type for $\varphi \in [0, 2\pi/F_k]$. Otherwise (two or more H intervals and E intervals), it is outside a bump. This suggests a way to decide about the reducibility of the quasi-periodic equation, by looking at the dependence in φ of the nearby periodic cases.

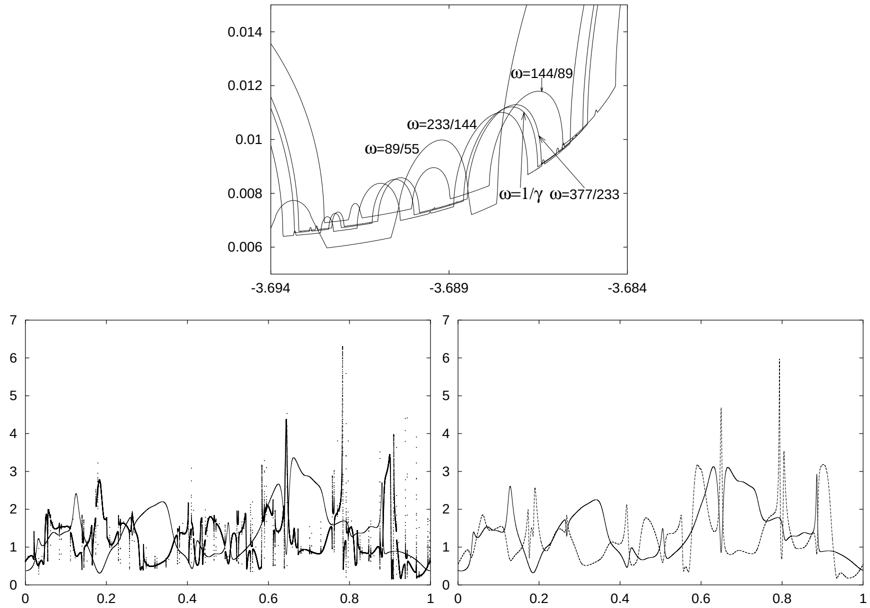

Figure 3. Top: Values of ℓ^2 for (9) as a function of λ_1 for $\lambda_2 = -4, e = 1, \omega = \gamma^{-1} = (1+\sqrt{5})/2$ and four approximants. Bottom left: $\mathrm{gf}^j(\varphi)$ versus $\varphi/(2\pi)$ for $\lambda_1 = -3.689$. gf^2 is plotted with dots. Bottom right: Same for $\lambda_1 = -3.694$. Both gf^j plotted with lines. See text for details.

Acknowledgements

Support by grants DGICYT BFM2000-805 (Spain), CIRIT 2001 SGR-70 (Catalonia) and partial support of grant INTAS 2000-221 is acknowledged. The computing facilities of the DS group at UB have been widely used.

References

1. H. Broer and C. Simó, *Bul. Soc. Bras. Mat.* **29** 253–293 (1998).
2. H. Broer, C. Simó and R. Vitolo, The Hopf-saddle-node bifurcation for fixed points of diffeomorphisms. In preparation.
3. P.M. Cincotta, C.M. Giordano and C. Simó, *Physica D* **182** 151–178 (2003).
4. G. Gómez, J.M. Mondelo and C. Simó, Refined Fourier analysis: procedures, error estimates and applications. Preprint 2001. Available at `http://www.maia.ub.es/dsg`.
5. F. Ledrappier, M. Shub, C. Simó and A. Wilkinson, Random versus deterministic exponents in a rich family of diffeomorphisms, *J. Stat. Phys.*, in press (2003).
6. J. Puig and C. Simó, Analytic families of reducible linear quasi-periodic equations. In preparation.
7. C. Simó, in *Global Analysis of Dynamical Systems*, ed. H. Broer, B. Krauskopf, G. Vegter, 373–390, IOP Pub., Bristol (2001).